Rolling Contact Fatigue on premium rail grades
Damage function development from field data

Hiensch, Martin; Steenbergen, Michaël

DOI
10.1016/j.wear.2017.10.018

Publication date
2018

Document Version
Accepted author manuscript

Published in
Wear

Rolling Contact Fatigue on premium rail grades: damage function development from field data

Martin Hiensch, Michaël Steenbergen

Delft University of Technology, Section of Railway Engineering, Faculty of Civil Engineering and Geosciences, Stevinweg 1, 2628 CN Delft, The Netherlands.

* e.j.m.hiensch@tudelft.nl

Abstract

The concept of the rail damage function provides vital understanding of the operational performance of rail grades in terms of surface degradation. The present study extends this concept from conventional to premium pearlitic rail. This is done on the basis of both simulations of dynamic train-track interaction and field observations. Rolling Contact Fatigue (RCF) damage index values for the conventional R260Mn and the premium R370CrHT grade rail are established, describing the behaviour of the associated damage functions. Defining the individual rail grade damage response to operational loading levels, the potential of the RCF-damage function to support the process of rail grade selection and track maintenance is further discussed.

Keywords: Rolling Contact Fatigue (RCF), wear, damage function, rail grade selection, premium rail

1. Introduction

Rail surface damage development and related costs of inspection and maintenance are a major concern to infrastructure managers. Control measures aiming to prevent or reduce damage development may target the wheel-rail interaction forces, limiting them through optimisation of the wheel-rail interface geometry or by stimulating the use of so-called track-friendly vehicles which produce reduced forces on the track. An alternative approach is the improvement of the material resistance to the imposed stress and slip levels. This line of approach is followed by the rail grade selection standards applied by most infrastructure managers, which specify more resistant rail grades to be installed at more demanding track sections such as curves. Beside the installed rail grade also the execution of maintenance measures (such as grinding or lubrication) can have a strong impact on the service life of rails [16]. This is supported by field experience, indicating that the expected benefit of improved steels has not generally been associated with a reduction in required maintenance. Based on the experience that rolling contact fatigue (RCF) became a problem only after the normal rail for a specific site was replaced by premium rail, Burstow [1] concludes that premium grade rail steels may not always be the best solution to prevent track damage and that careful consideration of track geometry, operating conditions and traffic is necessary when considering the most appropriate rail grade to select for use at a given location. Ref. [2] reports that the response of the rail grade with respect to RCF development depends on the track test conditions. Further understanding of rail grade performance as a function of operational loading conditions is therefore vital to support the process of rail grade selection. Rail damage models can be used as an asset management tool to analyse specific track sections, assessing the likelihood of RCF crack initiation and wear on the basis of given loading conditions.

In the literature, work has been undertaken to develop a simple parameter capable of describing damage development in terms of RCF as a function of the loading history. Burstow [3] has found the wear energy number (Tγ) to provide the best correlation between the output of RCF damage simulation work and observed crack location in the field. Tγ describes the mechanical energy dissipated in the wheel-rail contact patch, thus available for initiating damage at the contact surface on the rail. He presents a material specific damage function, derived from track inspections in combination with vehicle-track simulations. The function describes the relationship between the wear energy number and RCF crack initiation fatigue damage, by translating the calculated Tγ into a fatigue damage term, being the number of loading cycles to visual crack initiation. Currently this methodology has been applied only for analysis of sites containing the 'normal' grade rail R220 (according to the European norm [4]), although it can be expected that the concept itself works equally well for other material grades. There is however no validated damage model available for any other rail grade. In order to develop such models, the characterisation of different rail materials needs to be performed in terms of the Tγ loading history and related damage development. The objective of the present study is to establish the RCF damage functions for the normal R260Mn and premium R370CrHT grade rail. In analogy to ref. [3], the damage indices will be determined from track inspections in combination with vehicle-track simulations for the track sections under consideration.

The structure of this article is as follows: after the introduction, the theoretical framework is presented in chapter two, discussing rail RCF damage assessment in general. Chapters three and four contain the core of this work, with a discussion of the setup of field observations and vehicle-track simulations in the first chapter, and the relationship between results and track damage in the second chapter. Chapter five discusses the engineering relevance of damage function application in track design and maintenance, followed by conclusions in chapter six.

2. Assessment of RCF damage on rails in general

'Wear' is a damage phenomenon being inherently present in each rail-wheel contact, with surface material (oxides) being removed even at the lowest loading levels. Fatigue damage however will initiate only when the cyclic loading level exceeds the material fatigue limit. Assessment of the material response to cyclic loading can take place using so-called shakedown maps, presenting the material hardening curves that define the areas with different material response types in dependence to the peak Hertzian pressure, the material yield stress under pure shear and the traction coefficient [5]. Fatigue damage will develop when individual loading cycles result in the accumulation of plastic strains, exhausting the material resistance to further plastic deformation. This type of material response, known as plastic ratchetting, occurs when loading levels surpass the plastic shakedown limit. The development of fatigue damage at the surface can be slowed down or even entirely prevented by removal of material from the surface due to wear. The development of RCF at the rail-wheel interface depends therefore on the balance between crack initiation and wear rate. Fatigue crack initiation is governed by the process of ratchetting. The wear rate depends on the tangential force in combination with the occurring slip in the contact patch. Damage models incorporating the competing damage mechanisms of wear and fatigue crack growth can be used for the evaluation of rail wear and RCF initiation.

The damage energy model as developed by Burstow was first proposed in [6]. It describes the relationship between the wear energy number Tγ and RCF crack initiation fatigue damage. The parameter Tγ represents the work performed by the frictional shear stresses in the moving wheel-rail contact patch, usually considered per travelled unit distance along the track [15]. This performed work is equivalent to energy dissipated in the contact patch, and is commonly expressed for a unit length of 1 m, giving rise to Tγ being expressed in the unit [J/m] or [N]. The wear number Tγ is calculated from the sum of the lateral and longitudinal products of shear forces (T_x and T_y) and creepages (γ_x and γ_y) at the wheel/rail interface. The wear number is a standard output from vehicle dynamics software. From the model the calculated Tγ is translated into a fatigue damage index; the number of loading cycles to visual crack initiation. This 'RCF damage index' expresses the number of cycles before visible RCF cracks can be expected on the rail head. Burstow suggests, for reasons of feasibility, a minimum surface length of approximately 2 mm, stating that cracks to be visible at this length must have developed beyond the initiation stage and some crack growth must have taken place. For each contact location the fatigue damage from individual loading cycles can be summed using Miner's rule for variable amplitude fatigue loading [7]. When the fatigue life is exhausted, this results in visible RCF damage when the RCF damage index limit is reached.

The behaviour of the overall RCF damage function (shown at the bottom in Fig. 1) is determined by the individual linear damage functions regarding both wear and RCF (at the top in Fig. 1). At damage levels below the fatigue threshold (zone a) no RCF develops. For the rising slope of the damage function (zone b) RCF damage develops due to plastic ratchetting. At higher levels of energy dissipation the wear rate is seen to increase, removing RCF damage as indicated by the descending slope (zone c). When the damage function becomes negative (zone d), initiation of RCF damage is entirely suppressed by wear.

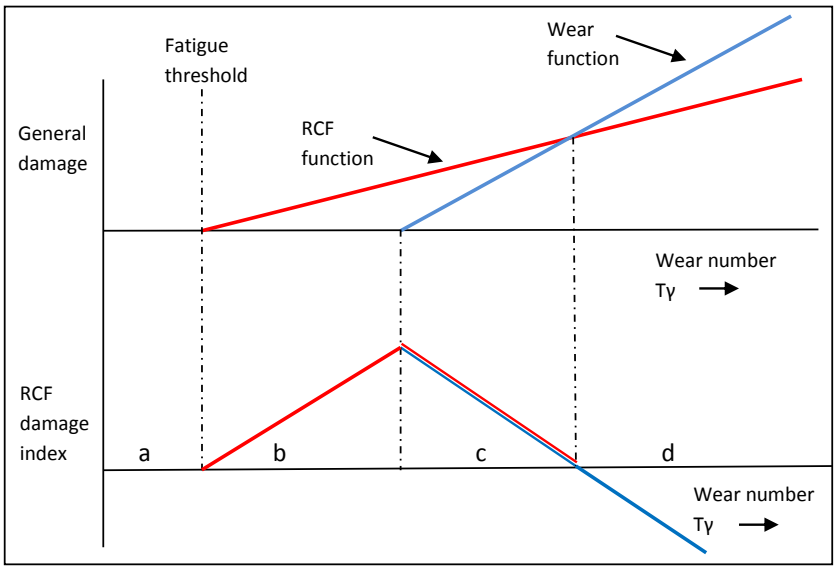

Fig. 1. Wear and RCF as competing mechanisms of rail surface degradation.

Wear mechanisms and transitions shape the course of the damage function. For rail materials these mechanisms have been studied by Bolton and Clayton with the help of two-disk testing [8]. To allow for a direct comparison between materials, Bolton and Clayton were the first to plot the wear rate against the wear number divided by the contact patch area (Tγ/A). From the occurring wear rate, the

contact surface appearance and the amount of wear debris occurring during the two-disk testing, three different wear regimes were identified. They were referred to as mild (type I), severe (type II) and catastrophic (type III), associated to increasing contact pressure and slip percentage. Examining side-worn rail samples from curved track sections, Bolton and Clayton conclude the type II wear regime to be most closely related to the rail crown and the gauge corner region, whereas type III wear is usually concentrated at the gauge face due to relatively high slip levels in flange contact. Burstow [3] associated mild wear to the RCF-dominated regime (the rising part of the damage function in figure 1), with the transition from mild to severe wear to the change to the wear-dominated regime (the falling part). Lewis et. al [9, 10] suggest this mild to severe transition to be associated with the onset of full sliding contact conditions.

Burstow [6] has demonstrated that the RCF damage index methodology can predict the damage level quite well when applied to sites where the RCF generating forces are determined by track irregularities and quasi-static curving. However, in the development of the model a number of assumptions have been made. Burstow mentions the limited number of applied wheel profiles as well as his use of only one single vehicle model, restricting the distribution of contacts and loading conditions. Also the condition of the track geometry at the time of the site survey has been assumed constant over its entire service life. These assumptions will affect the reliability of the model. Nonetheless, good correlations are reported between predictions and field observations of track sites with RCF.

3. Set-up of the damage function determination

In order to derive RCF damage functions for different rail grades, results from track inspections have been assessed in combination with results of vehicle-track simulations for the considered cases. Damage index values have been determined from the accumulated damage to the first visible RCF cracks. In this paragraph the successive individual steps of the analysis are discussed.

3.1. Field observations

Two track sites were selected, denoted here as site A and B. Track geometry details are presented in Table 1. The maintenance history of both sites shows that they are susceptible to the formation of RCF in the form of headchecking. From the difference in curve radii and installed cant between these sites different operating Ty values are to be expected. This allows for the determination of a wider damage index range in the damage function. For purpose of comparison both sites were visually inspected prior to rail replacement. The RCF development at site A (Fig. 2) was found uniformly distributed over the entire curve. At site B, in the part of the curve with a constant radius, RCF was not uniformly distributed but clustered in ‘patches’. This suggests a variation in local contact stresses, likely associated to track geometry. At the high rail of both sites A and B, two different rail grades were installed in series; the normal grade R260Mn and premium grade R370CrHT, with a length of 180 m length each. A monitoring program was started from the moment the new rail was installed. During the first year, this comprised visual inspection of the running band each second month, along with measurements of hardness, rail profile and crack depth (eddy current). After the first year the inspection interval was extended to four months.

Table 1.
Track geometry details (*partly 1200m)

	Site A	Site B
Curve radius (m)	1000*	2450
Cant (mm)	80	60
Max. Speed (Km/h)	120	140
Length full curve (m)	1200	1150
Avg. daily tonnage (.10^3t)	31.5	48.1

Since the RCF crack initiation model applies damage summation, it requires loading information in terms of the composition of the daily passing rolling stock. To this purpose strain gauges were installed in the track, measuring the number of passing axles, the axle loads and the train speed. From the recorded wheel base and bogie spacing for each passing vehicle also the vehicle type could be identified.

Fig. 2. High rail running surface at site A – situation prior to rail replacement (traffic direction to the right; depicted rail length about 0.36 m).

3.2. Vehicle dynamics simulations

Train registrations clearly showed the loading at both sites to be dominated by the same three train types; two passenger intercity trains and a particular freight configuration, together representing 70% of all axle passages and born tonnage. Although not serving the same route, the train type distribution for both sites was similar. The three dominant vehicle types were modelled using the simulation software VAMPIRE® Pro 6.30. The main dynamic parameters for the two operating passenger vehicles are listed in the annex of this paper (table 3). The main parameters of the freight vehicle are presented in ref. [14]. Vehicle dynamics simulations were performed for quasi-static curving conditions, based upon the track geometry design values. Further dynamic simulations were performed for the track with irregularities as measured by a recording train during the period of field testing. Because of the fact that the wheels of passenger vehicles are frequently reprofiled, vehicle simulation runs were performed with the new (unworn) S1002 wheel profile. Freight vehicle

simulation runs were performed with an average worn S1002 wheel profile, selected from profile measurements performed at a number of freight wagons in service. The rail inclination was set to 1:40 and the design track gauge was 1435 mm. The applied rail profile was UIC 54E1 as defined in the norm [4]. The coefficient of wheel-rail friction was set to f=0.32. This is a representative value in accordance with ref. [13], which specifies the assessment of the running characteristics of railway vehicles for the European network. The vehicle speed and loading condition to be applied in the simulations were derived from the strain gauge measurement results. The vehicle speed was set identical for both passenger train types; 120 km/h at site A and 130 km/h at site B. The freight train speed for both sites was 90 km/h. No traction was applied. Simulations for all vehicle types were carried out in loaded condition. As mentioned earlier the selected three vehicle types together establish 70 percent of all axle passages and born tonnage. The remaining 30 percent of the total tonnage, mainly from different commuter train types, has been included in the simulations by simply adding their tonnage to that of the two dominant passenger train types.

3.3. Damage summation

The considered damage loading period started at the moment of rail renewal, ending at the moment of first visible RCF crack detection with a minimum surface length of approximately 2 mm. For the total number of vehicles of each type that has passed the considered site during this period, the Tγ damage summation is performed for each wheelset on each vehicle. Summation of the damage has been carried out with respect to the position in the curve (x), the contact position on the rail head (y) and the contact patch area and ratio (a/b).

4. Test results and implementation in the damage model

The results of track inspections, vehicle dynamics simulations and damage summation are presented in this section, together with the interpolated part of the damage function that follows from this input. Subsequently, the further behaviour of the damage function for premium rail is extrapolated on the basis of work performed by Bolton and Clayton [8] regarding rolling-sliding wear.

4.1. Field observations

From the inspection, a clear difference in the accumulated tonnage until visible crack initiation could be established between the normal and premium rail grade, as can be seen in Table 2.

Table 2.
Accumulated tonnage to visible crack initiation for different measurement locations

	Accumulated tonnage until visible crack initiation (.10^6 ton).	
	Track site A	Track site B
R260Mn	5,8	8,8 (750m)*
R260Mn	n.a.	14,5 (430m)*
R370CrHT	20,1	35,0 (540m)*
R370CrHT	11,9	33,5 (990m)*

*) relative position of the measurement location, corresponding to travelled distance (m) as presented in figure 5.

Shortly after installation the premium rail grade is observed to develop a fine network of superficial cracks (‘craquelure’, Fig. 3). However, visible cracks that develop beyond the initiation stage are

found on the premium grade at a much later stage. At site A, RCF develops uniformly over the entire section, independent of the rail grade. Differences in the delay until RCF initiation at site A were dominated by the rail grade but also a difference between the two R370CrHT locations is observed. Similar to the situation prior to rail replacement, RCF at site B develops more locally, with damage clustering in patches. At site B, differences in the delay until RCF initiation were found to depend on rail grade and the position in the curve. Visible headcheck development is illustrated in Fig. 4. Eddy current measurements indicate these cracks to be about 0,3 to 0,4 mm in depth. From profile measurements performed 18 months after rail installation the premium rail grade at track B showed hardly any wear nor deviation from the design profile, confirming a mild wear operating regime.

Fig. 3. Fine network of superficial cracks (craquelure) on the premium rail grade (site B). Direction of traffic is to the left, depicted rail length is about 0.1 m.

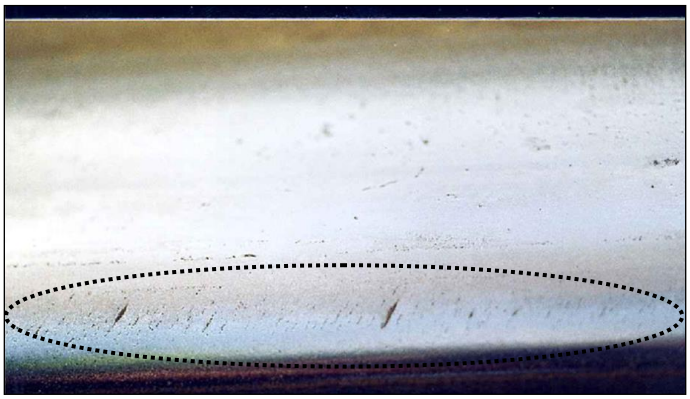

Fig. 4. Visible headchecking at the rail shoulder (within indicated zone, approx. 3 to 5mm in length), site B, grade R370CrHT. Direction of traffic is to the left, depicted rail length is about 0.1 m.

4.2. Vehicle dynamics modelling

For the purpose of this study only results at the high rail are evaluated, both for the design track geometry (quasi-static curving conditions) and for the situation with measured track irregularities. For site A the most striking result is that, apart from the leading wheels of the bogies from both passenger type vehicles, none of the other vehicle contact positions during quasi-static curving surpass the fatigue crack initiation limit value of the R220 damage function. Neither the freight vehicle nor the trailing wheels of the passenger vehicles seem to contribute to the observed RCF damage at this site. Evaluating vehicle dynamics in relation to curving behaviour with track

irregularities, Tγ development for site A does not show local variations and the average level is equal to the quasi-static curving. At site B the Tγ loading levels for quasi-static curving are below - or just touch - the R220 fatigue crack initiation limit for all vehicle type contact positions, suggesting no significant RCF damage development (Fig. 5a). However, when evaluating vehicle dynamics with measured track irregularities the track geometry variations result in a local steep increase of Tγ, surpassing the threshold value at a number of track segments (Fig. 5b). Further evaluation shows this increase to be due to especially lateral irregularities and a number of a sharp local deviations in the curve radius. For site B, Tγ loading levels vary distinctly due to the track geometry variations; therefore damage summation for this curve should be position-dependent. From Fig. 5 the general Tγ level during quasi-static curving and the level during curving for the measured track geometry are seen to differ, mainly due to differences between design and measured cant.

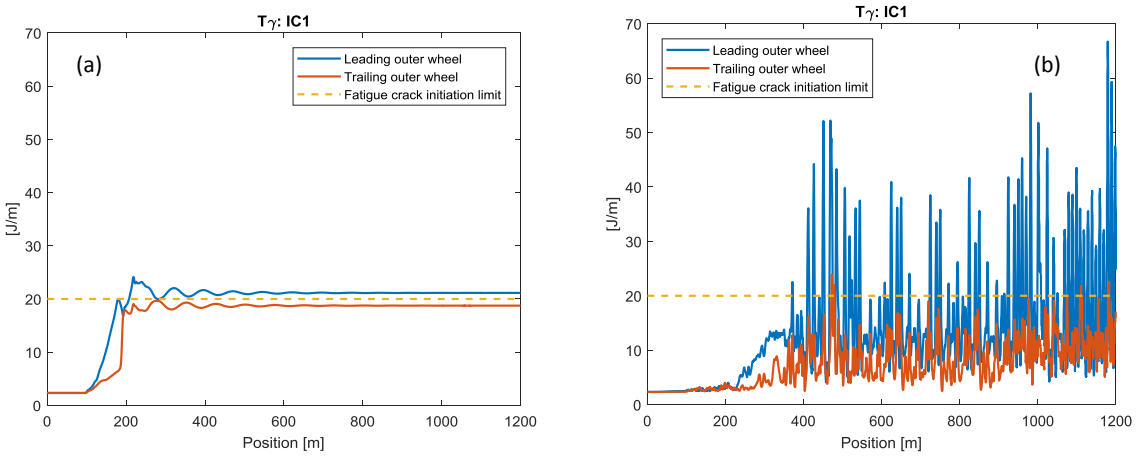

Fig. 5. Tγ development of the IC1 passenger type vehicle at the first 1000m of site B during quasi-static curving (a) and for the situation including variations in track geometry (b).

4.3. Damage summation

The contact patch area and its location on the railhead are evaluated for the outer wheels and compared to the location where RCF initiation is observed. At track site A, both for quasi-static curving and for curving behaviour with track irregularities, the railhead contact positions of the leading outer wheels of both passenger vehicles correspond to the RCF initiation area. This indicates that the fatigue damage from the individual loading cycles can be summed and related to the observed damage. The observed running band and calculated wheel-rail contact positions are presented within Fig. 6. During quasi-static curving the contact patch locations of the two intercity type vehicles remain unchanged, each represented in Fig. 6 by one shaded marker. For the curving situation with measured track geometry both passenger vehicles show a spread in contact conditions due to the presence of track geometry variations. This is illustrated by two shaded markers for each train, designating the extremities of the contact band.

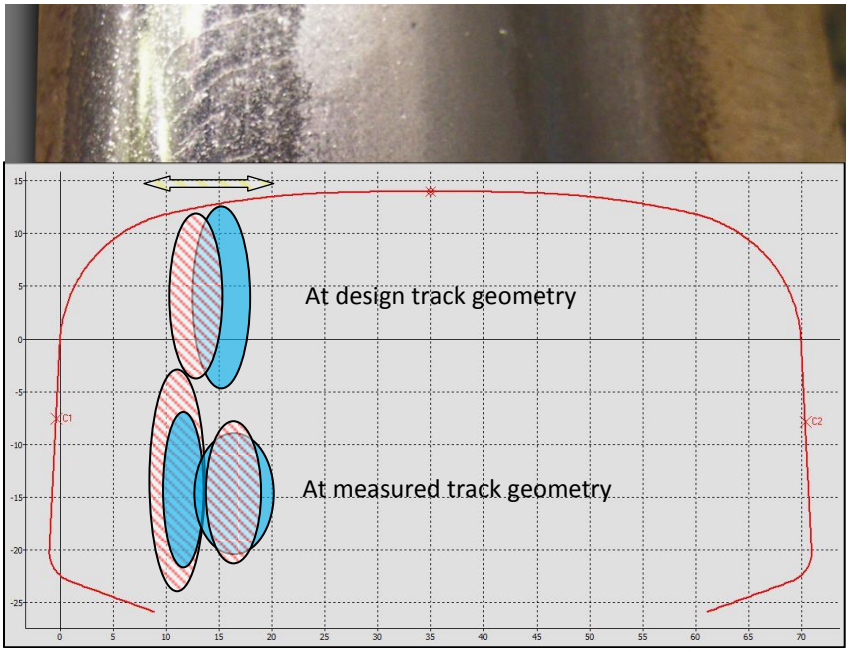

Fig 6. Site A, R260Mn, 21 months after installation – detail of the running band with arrow indicating the position of the observed RCF damage. The calculated contact location and size at the extremities of the contact band for the leading wheels of both passenger type vehicles are marked for the quasi-static curving condition and for the situation with included track geometry variations.

At site B, wheel-rail contact at the RCF initiation zone only occurs for a discrete number of positions throughout the curve. These coincide with major local deviations in lateral alignment and in curve radius. The observed shifting of the contact location towards the rail shoulder results in a sharp local increase of Tγ for all evaluated vehicle types, as visible in Fig. 5b. These locations were found to be the first ones where RCF damage started to develop. The contact patch distribution for the vehicle response to track geometry variations indicates that only the leading wheels contribute to the observed head check generation.

4.4. Damage function development - interpolation

Damage function indices for the different rail grades have been determined from the observed period to RCF damage initiation in combination with calculated Tγ loading levels, loading positions and corresponding loading frequencies. Tγ levels for quasi-static curving conditions were applied to site A. For site B, Tγ levels were applied from simulations including track irregularities. The resulting indices are presented in Fig. 7 as a function of the wear number. The square (□) box markers indicate the established R260Mn behaviour. The diamond (◊) shape markers denote this dependency for the R370CrHT rail grade. The RCF damage function as established by Burstow [6] for the here presented section is shown by the black line. The dotted line represents the established R370CrHT damage function within this area. The damages indices obtained for the R260Mn rail grade can be observed to coincide with the RCF damage function of R220. This is in accordance with observations made by Zacher [11], who showed that gauge corner cracking predictions based upon the R220 damage function matched remarkably well to that of the R260 grade rail. These findings further support the

conclusion that the RCF regime of the R220 damage function can be applied to the entire family of normal pearlitic rail grades including R260 and R260Mn.

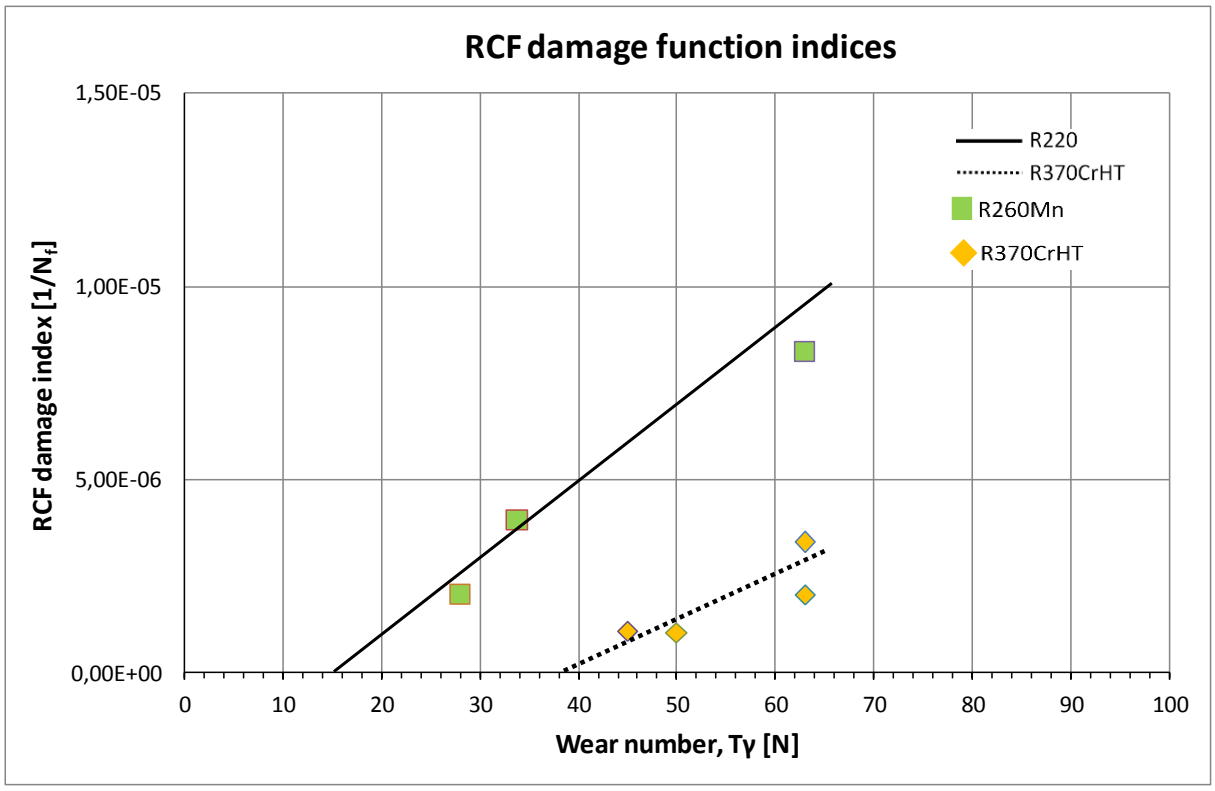

Fig. 7. RCF damage index values for the normal R260Mn and premium R370CrHT grade rail as a function of the wear number, derived from site A and B. The black line represents the ascending part of the R220 damage function from Burstow [6]. The dotted line represents the established R370CrHT partial linear damage function.

The observed spread in accumulated tonnage until visible crack initiation for R370CrHT rail grade at site A, as shown in Table 2, and the related spread in the RCF damage index value for the calculated wear number can be explained from locally varying operational conditions. Changes in track geometry developing over time are expected to lead to larger deviations of the quasi-static Ty levels calculated for site A as compared to site B, for which track geometry variations were included from the beginning. Also the Ty level at site A is situated near the expected peak of the damage function, which means that both a periodical decrease or increase of Ty will lead to an increase in accumulated tonnage until visible crack initiation. At site B, situated in the rising part of the function, the effect of Ty fluctuations on accumulated tonnage until visible crack initiation will be more levelled off. Moreover, accuracy can also be affected by the chosen inspection interval and seasonal influences.

4.5. Damage function development – extrapolation

The expectation for the remaining part of the damage function can be based on the work performed by Bolton and Clayton [8] regarding rolling-sliding wear damage. The fatigue crack initiation limit, the starting point of the rising slope, is determined by the mechanical properties to resist fatigue initiation. Ponter [5] shows the shakedown limit above which fatigue damage will develop depends

on the material yield strength in shear. From its higher yield shear strength and resulting higher shakedown limit an increase in the RCF initiation limit wear number value can be expected for R370CrHT as compared to R220. The starting points of the individual damage functions in Fig. 7, as determined from the established index values, confirm this expected behaviour. Burstow [3] associates mild wear with the rising part of the damage function. For the type I mild wear regime Bolton and Clayton find the wear rate to be independent on examined rail steels. This indicates the ascending slope of the damage function for the different materials to be determined by its early stage RCF crack growth properties. Garnham and Davis [12] conclude the prior-austenite (PA) grain boundary dimensions and shapes to play a significant role with respect to initial RCF crack initiation growth rates, particularly if defined by regions of pro-eutectoid (PE) ferrite. With initial crack propagation restricted to the boundaries of the deformed PA grains at the surface, microstructural properties define this very early crack growth behaviour. Premium rail grades are characterized by a low level of intergranular ferrite. Microstructure crack-retarding properties of premium rail are further optimised through a very small lamellar spacing achieved by heat treatment. Small cracks (during initiation and first stages of crack growth) are sensitive to lamellar spacing, since the lamellar structure possesses excellent crack-retarding properties thereby decreasing the transgranular crack growth rate. The less steep ascending slope of the R370CrHT damage function reflects its improved crack delaying properties and improved resistance to plastic deformation as compared to the normal grade rail. With RCF crack initiation increasingly suppressed with increasing wear rate Burstow [3] associates the transition from mild to severe wear with the transition from the RCF to the wear regime, the peak of the damage function. For the type II wear rate, Bolton and Clayton have found considerable differences between the various rail steels and concluded these to be dependent on the intrinsic material properties. The type II wear rate for the individual rail steels are found to be a linear function of $T\gamma/A$. The reduction factor in wear rate was observed to increase with increasing material hardness, indicating a less steep descending slope of the R370CrHT material damage function as compared to R220. To a lesser extend this also seems to apply to R260Mn. The exact geometry of the descending slope of these rail grades however needs to be further defined and validated.

The transition from type I to type II wear occurs at operational conditions well beyond the fatigue crack initiation / shakedown limit. This transition seems to be determined by the level of the frictional work destroying the protective oxidation layer and to a lesser extent by the resistance to plastic deformation. Since the oxidation rates of normal and premium rail grades are expected to be relatively similar, one may speculate the transition zone creepage value of these grades to be in the same order. This expected behavior is confirmed by presented transition zone creepage values by Bolton and Clayton [8]. At contact stresses typical for moderate curving (1300 MPa, [12]) these show little to no difference for the different rail materials, indicating under these conditions the damage function peak for all examined rail grades to be positioned at a similar wear number. These insights can be used to further estimate the R370CrHT damage function within the regimes of simultaneous RCF-wear and of full wear. Fig. 8 presents the individual R220 damage functions derived from Burstow [6] together with those determined for R370CrHT. The starting point of the RCF function is determined by the mechanical material properties to resist fatigue initiation, whereas the slope reflects the early stage RCF crack growth properties. Transition from the regime of RCF to wear is assumed to start at the same $T\gamma$ level for both materials with the slope of the descending wear

function proportional to the hardness. Since the type II wear function is not yet defined, the starting point and geometry of the descending branch of the R370CrHT damage function remain speculative.

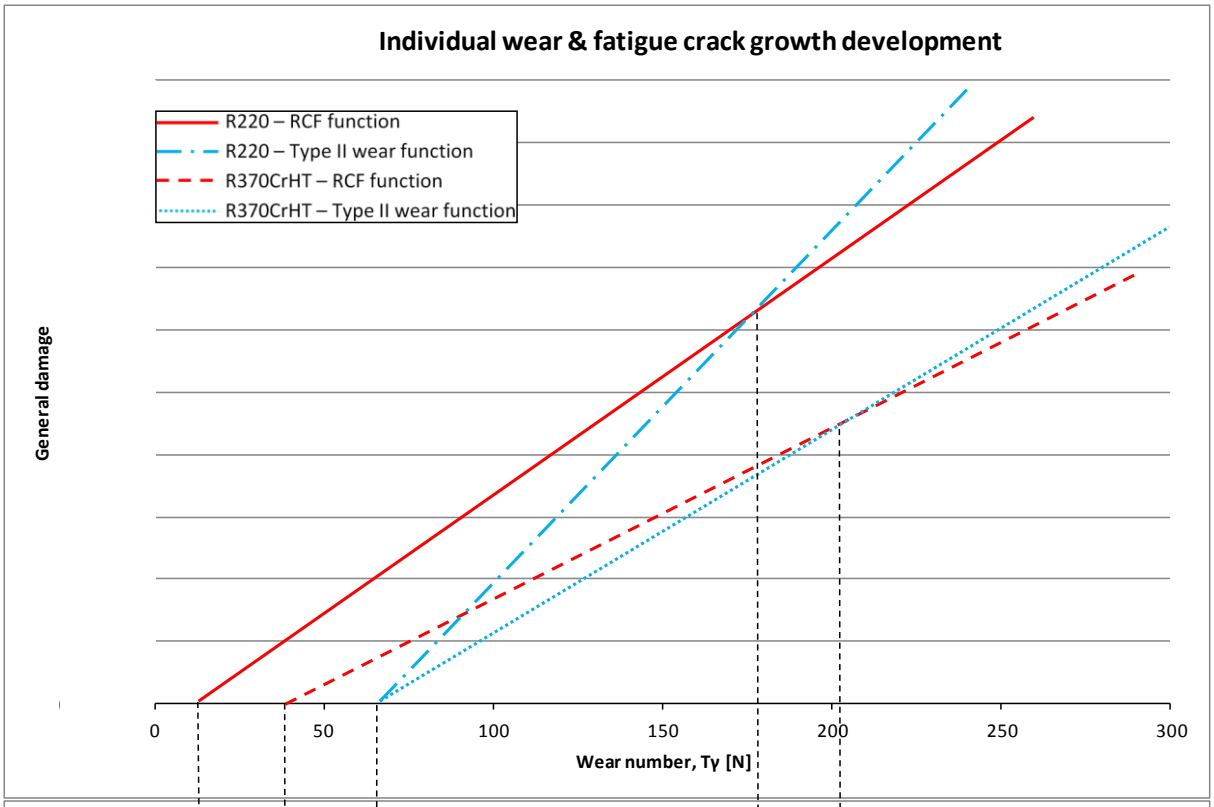

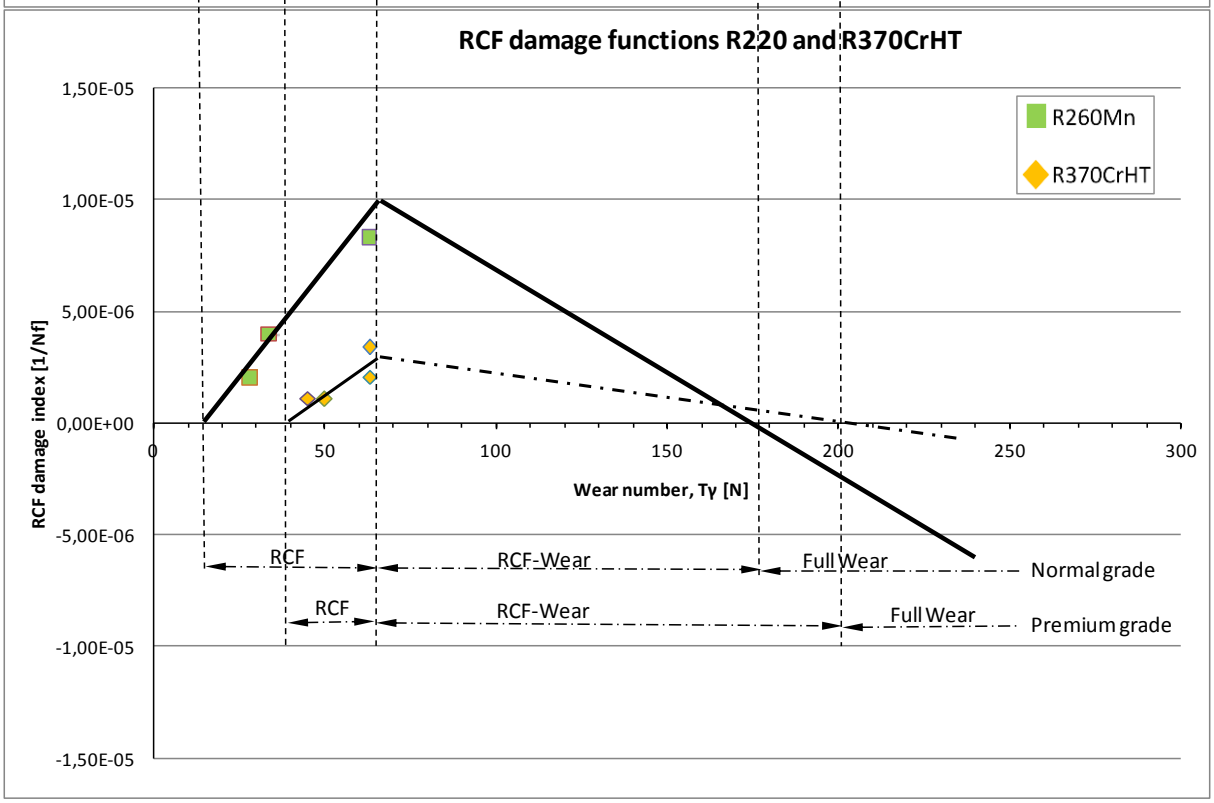

Fig. 8. The individual wear and fatigue crack growth development for R220 as derived from Burstow [6], together with those for R370CrHT as determined in this study (top); RCF damage functions for both R220 and R370CrHT rail grades (bottom). The starting point and development of the downward slope of the R370CrHT damage function (stripe-dotted line) remain speculative.

5. Discussion: engineering relevance and outlook

The R370CrHT RCF damage function has implications with respect to rail grade selection in design situations. Compared to the normal grade, the increased fatigue crack initiation limit value of the R370CrHT damage function indicates a reduction in RCF susceptibility, preventing RCF initiation for an extended range of track curving conditions. The reduced slope of the ascending part of the R370CrHT damage function will, under equal loading conditions, result in a significant increase in expected time to visible RCF damage initiation as compared to normal grade rail. Although not validated, the reduced RCF index peak value will have a further beneficial effect on the loading frequency until visible RCF.

Wear number (Tγ) loading levels and frequencies for any particular site are required in order to apply the RCF damage function to select the optimal rail grade to be installed or to forecast headcheck development. A daily fatigue index as suggested in [11] can be used by the track engineer, to consult e.g. through look up tables. The Tγ magnitude is found to depend strongly on the curve radius together with vehicle curving characteristics. The contact patch distribution at the evaluated conditions, affecting damage summation, indicates that only leading wheels contribute to the damage summation. Especially at the examined larger radius curve (R=2500 m) the operating Tγ levels and contact patch distribution are significantly influenced by the intensity of track geometry variation. This behaviour needs to be reflected within the track-train specific look up and can be addressed for example by taking into account the (mean) track quality number as obtained by the track geometry recording train. Due to the wide range of influencing factors (e.g. wear of wheel profiles, friction conditions), the accuracy of the theoretical model is valuable only to a certain extent. To support rail grade selection in practice an overall description of the RCF damage function for the different rail grades therefore seems to be sufficient.

RCF damage models can support rail grade selection, switch design and rail maintenance planning. Using these models, the damage response of different rail grades can be predicted given the dynamic loading conditions. Accordingly, measures can be taken e.g. avoiding operational Ty values within the RCF damage regime. The mean value of the wear number along a curve or switch section can be used to optimise track maintenance in relation to RCF generation. With the applicable RCF damage function the accumulated fatigue index for the section can be determined from the average daily traffic. This can support e.g. the planning of maintenance activities such as grinding or rail grade selection upon renewal. Damage models can also be used in an engineering environment to assess the impact of changes in train operation (e.g. increased train speed, vehicle types, axle loads) on the expected damage development and, consequently, required maintenance.

6. Conclusion

On the basis of a combination of dynamic train-track simulations and regular track inspection results, RCF damage index values have been established for both the normal R260Mn and the premium R370CrHT heat treated pearlitic rail. From these index values the rising RCF-branch of the damage functions of both rail grades has been established. RCF damage index values for R260Mn were found to coincide with the RCF damage function of the R220 grade as reported in the literature by Burstow [6]. In line with work by Zacher [11] these findings support the conclusion that the RCF regime of the R220 damage function, with Tγ values in the domain between the fatigue crack initiation limit and the peak value of 65 N, is applicable to the entire family of normal pearlitic rail grades, including R260 and R260Mn. Compared to the normal grade, the established part of the R370CrHT damage function shows an increased fatigue crack initiation limit value together with a reduced slope of the rising part of the function.

It can be concluded from the established part of the R370CrHT damage function that application of this grade in the type I mild wear regime is beneficial to avoid RCF. The increased crack initiation limit will extend the track length for which no RCF initiation is expected. Within the RCF regime itself the initiation of headchecking will require an increased number of loading cycles. Within the operational window of the RCF damage function with Tγ values below 65 N, the application of premium grades such as R370CrHT can therefore be expected to result in a significant reduction of the maintenance need.

The quantitative determination of the descending part of the damage function for premium grade rail requires further research. A difficulty here is the wide range in operational loading conditions (e.g. due to variation in vehicle type, wheel profiles, vehicle speed, traction and adhesion levels). To obtain more controlled conditions, laboratory two-disk testing could be applied to both establish and validate the damage functions for the different materials.

The RCF damage functions have significant engineering relevance. Their application allows for a dedicated rail grade selection, adapted to site-specific operational conditions. They can be used either in plain track and in the design of special parts of the rail network, such as switches and crossings. Assessment of the Wear number (Tγ) loading levels and frequencies for a particular site provides careful consideration when selecting the most appropriate rail grade for use at a given location, assisting the track engineer towards a fit-for-purpose decision. This can be expected to significantly affect the life-cycle costs.

Acknowledgements

This research is being carried out under the project number T91.1.12475a, in the framework of the Research Program of the Materials innovation institute M2i (www.m2i.nl). Part of the work was funded by ProRail (the Dutch rail infra management organisation). The authors would like to thank Nico Burgelman for his support regarding the simulation work, preparing the run-files and the output.

References

[1] Burstow M. Experience of premium grade rail steels to resist rolling contact fatigue (RCF) on GB network, Ironmaking & Steelmaking (2013), 40:2, 103-107.

[2] Stock R, Pippan R, RCF and wear in theory and practice – The influence of rail grade on wear and RCF, Wear 271 (2011) 125-133.

[3] Burstow M. Whole Life Rail Model Application and Development for RSSB (T115) – Continued Development of an RCF Damage Parameter, in Engineering Research Programme 2004, Rail Safety & Standards Board.

[4] NEN-EN 13674-1:2011, Railway applications - Track - Rail - Part 1: Vignole railway rails 46 kg/m and above.

[5] Ponter ARS et al. Application of the kinematical shakedown theorem to rolling and sliding point contacts, J. Mech. Phys. Solids Vol. 33, No. 4, pp. 339-362, 1985.

[6] Burstow M. (2003) Whole Life Rail Model Application and Development for RSSB – Development of an RCF Damage Parameter, AEATR report, AEATRES- 2003-832 Issue 1, October 2003.

[7] Miner AM, Cumulative damage in fatigue J. Appl. Mechanics, 12 (3) (1945), pp. A-159.

[8] Bolton PJ, Clayton P. Rolling-sliding wear damage in rail and tyre steels, Wear, 93 (1984) 145-165

[9] Lewis R, Olofsson U. Mapping rail wear regimes and transitions, Wear 257 (2004) 721-729

[10] Lewis R, Dwyer-Joyce RS. Wear mechanisms and transitions in railway steels. Proc. IMechE, Part J: Engineering Tribology, 2004, 218, 467-478.

[11] Zacher M. Prediction of gauge corner cracking in rails for rail maintenance, Contact Mechanics, CM2009, Florence, Italy.

[12] Garnham JE, Davis CL. Very early stage rolling contact fatigue crack growth in pearlitic rail steels, Wear 271 (2011) 100-112.

[13] EN 14363:2016, Railway applications. Testing and Simulation for the acceptance of running characteristics of railway vehicles. Running Behaviour and stationary tests.

[14] Molatefi M, Hecht M, Kadivar MH. Critical speeds and limit cycles in the empty Y25-freight wagon, Porc. IMechE Vol. 220 Part F: JRRT67, 2006.

[15] Alarcón GI, Burgelman N, Meza JM, Toro A, & Li Z. The influence of rail lubrication on energy dissipation in the wheel/rail contact: a comparison of simulation results with field measurements. Wear, 330, (2015) 533-539.

[16] Steenbergen JMM, Rolling contact fatigue in relation to rail grinding, Wear356-357(2016)110–121

Annex

Table 3.
The main dynamic parameters for the two operating passenger vehicles.

Mass - metric tons (MT)		**IC 1**	**IC2**
Car body secondary mass			
Tare	MT	30	38
Laden	MT	35	46
Crush	MT	40	49
distance between bogie pivots	m	19	20
Centre of gravity (laden)			
CG long. offset	m	0,06	0,11
CG lat. Offset	m	0,01	0,01
CG height above rail	m	1,98	2,25
Primary suspension mass			
Bogie (motor)	MT	2,6	3,3
Wheelset	MT	1,7	1,7
longitudinal offset wheelset	m	2,5	2,5
CG height above rail	m	0,5	0,5
Wheel radius (new)	m	0,46	0,46
Wheel radius (fully worn)	m	0,42	0,42
Wheelset roll/yaw inertia	MTm^2	0,8	0,8
Primary vertical dampers			
Linear rate	(MNs/m)	0.027	0.025
distance primary damper to pivot	m	0,6	0,7
Primary suspension			
longitudinal stiffness	(N/m)	4*10e7	4*10e7
vertical stiffness	(N/m)	1.15*10e6	1.15*10e6
Airspring stiffness (laden) linear	MN/m	0,388	0,413